

2-Dimensional Kinematics of Simulated Disc Merger Remnants

Roland Jesseit¹*, Thorsten Naab¹, Reynier Peletier² and Andreas Burkert¹

¹ Universitäts Sternwarte München, Scheinerstr. 1, D-81679 München, Germany

² Kapteyn Astronomical Institute, University of Groningen, PO Box 800, 9700 AV Groningen, The Netherlands

Draft version. Accepted ??. Received ??? in original form ???

ABSTRACT

We present a two-dimensional kinematic analysis for a sample of simulated binary disc merger remnants with mass ratios 1:1 and 3:1. For the progenitor discs we used pure stellar models as well as models with 10% of their mass in gas. A multitude of phenomena also observed in real galaxies are found in the simulations. These include misaligned rotation, embedded discs, gas rings, counter-rotating cores and kinematic misaligned discs. Using the 2D maps we illustrate projection effects and the change in properties of a merger remnant when gas is included in the merger. We find that kinematic peculiar subsystems are preferably formed in equal mass mergers. Equal-mass collisionless remnants can show almost no rotation, regular rotation or strong kinematic misalignment. The inclusion of gas makes the remnants appear more round(1:1) and axisymmetric(3:1). Counter-Rotating Cores (CRCs) are almost exclusively formed in equal-mass mergers with a dissipational component. 3:1 remnants show a much more regular structure. We quantify these properties by applying the kinematic methods recently developed by Krajnović et al. This work will help to understand observations of elliptical galaxies with 2D field spectrographs, like SAURON and Sinfoni.

Key words: methods: analytical – methods: N-body simulations – galaxies: elliptical and lenticular, cD – galaxies: formation – galaxies: evolution – galaxies: fundamental parameters – galaxies: kinematics and dynamics

1 INTRODUCTION

Elliptical galaxies are generally believed to form from major mergers of galaxies with mass ratios $\eta \leq 4 : 1$ (?). While early models investigated preferentially mergers of disc galaxies (e.g. ?, ?), that also very likely contained gas, it has become clear more recently that massive ellipticals are a result of collisionless early-type mergers or mixed mergers (?). Up to now, data on the kinematic structure was often restricted to their apparent major axis, leading to severe restrictions for a detailed quantitative analysis and comparison with theoretical models. This situation has changed recently with the successful operation of SAURON, an integral field spectrograph (?; ?) that by now has provided high quality two-dimensional(2D) kinematic data of a representative sample of early-type galaxies. This data allowed to identify many kinematic features from a 2-dimensional view of a galaxy. Among these features are kinematically decou-

pled cores, counter-rotating discs, depressions of the central velocity dispersion, strong kinematic misalignment and others. In addition, 2-dimensional data is uniquely suited to constrain models of the internal stellar dynamical structure of these galaxies. These models in turn are an important tool to determine the Mass-to-Light ratios of early-type galaxies (?).

The 2D SAURON observations place important new constraints on the formation process of elliptical galaxies which should be compared with theoretical models. Surprisingly, 2D kinematic analysis of simulated merger remnants has been given little attention in the past. ? showed 2D maps of a few collisionless merger remnants and identified some global properties like kinematic misalignment and central velocity dispersion dips.

In this paper we will present the analysis of a large sample of 1:1 and 3:1 disc merger remnants with and without gas (?). Gas mergers are motivated by a recent study of ?, henceforth NJB06, who have shown that dissipation must have played an important role at least in the formation of low luminosity giant elliptical galaxies, in particular

* E-mail: jesseit@usm.uni-muenchen.de;naab@usm.uni-muenchen.de; peletier@astro.rug.nl;andi@usm.uni-muenchen.de

to explain the shape of the line-of-sight-velocity-distribution (LOSVD), which can not be reproduced by collisionless remnants. For a quantitative analysis we will use a recently developed method termed *kinometry* (?; henceforth K06). Kinometry in analogy to photometry determines the geometrical features of projected iso-velocity contours like their shape and position angle. In principle this method can also be applied to higher moments of the LOSVD, but we will focus on velocity and velocity dispersion maps. This is the first application of kinometry to simulated galaxies.

In the course of this work we will compare merger remnants of collisionless progenitors and progenitors that contained gas which were formed by the same merging symmetry. We can therefore study *in situ* how the inclusion of gas modifies the velocity structure of a simulated galaxy. In Section 2 we introduce the simulation sample. We explain the observational method to obtain 2D maps of various moments of the LOSVD in Section 3. The maps and their kinematic analysis are presented in Section 4. We compare these results to 2D-kinematics of observed galaxies in Section 5 and summarize our findings in Section 6. Velocity maps and kinometry of the whole sample are shown in the Appendix.

2 SIMULATIONS

The collisionless simulations are a subset of the simulations discussed in detail by NB03. The simulations with gas, which we use for our analysis are identical to the ones presented in NJB06. In the following we give only the most important simulation parameters:

The progenitor disc galaxies were constructed in dynamical equilibrium using the method described by ?. The system of units was: gravitational constant $G=1$, exponential scale length of the larger disc in the merger $h_d = 1$ (the scale height was $h_z = 0.2$) and mass of the larger disc $M_d = 1$. The discs were exponential with an additional spherical, non-rotating bulge with mass $M_b = 1/3$, a Hernquist density profile (?) and a scale length $r_b = 0.2h$, and a pseudo-isothermal halo with a mass $M_d = 5.8$, cut-off radius $r_c = 10h$ and collisionless core radius $\gamma = 1h$. The parameters for the individual components were the same as for the collisionless mergers presented in ?. For this study we have re-simulated the full set of 1:1 and 3:1 mergers with an additional gas component in the disc. We replaced 10% of the stellar disc by gas with the same scale length and an initial scale height of $h_{z,gas} = 0.1h_z$. This is in agreement with recent results from ? in which they show that merging progenitor galaxies at low redshifts contain on average 10% gas for ellipticals more massive than 10^{10} solar masses. The gas was represented by SPH particles assuming an isothermal equation of state, $P = c_s^2 \rho$, with a fixed sound speed of $c_s = 0.039$ in velocity units corresponding to $c_s \approx 10 \text{ km/s}$ if scaled to a Milky Way type galaxy. The N-body/SPH simulations were performed using the hybrid N-body/SPH tree code VINE (Wetzstein et al. in prep.) with individual time steps.

The galaxies approached each other on nearly parabolic orbits, in agreement with predictions from cosmological simulations (?), with an initial separation of 30 length units and a pericenter distance of 2 length units. The inclinations of the two discs relative to the orbit plane were i_1 and i_2 with

Table 1. Properties of the modeled merger remnants. Special kinematical features observed and initial orientations of the progenitor discs are shown.

Model	comment	i_1	i_2	ω_1	ω_2
11C3	regular rotation	0	0	71	-30
11C5	low rotation	-109	-60	180	0
11C8	surface density change	-109	-60	71	90
11C12	kinematic misalignment	-109	0	71	90
31C6	regular rotation	-109	-60	71	30
11S2	ring-like depression in σ	0	0	71	30
11S6	KDC, counter rotation	-109	-60	71	30
11GS6	high σ gas disc	-109	-60	71	30
11GS9	polar ring	-109	0	180	0
31GS19	low σ disc	0	0	71	-30

arguments of pericenter ω_1 and ω_2 . In selecting unbiased initial parameters for the disc inclinations we followed the procedure described by ?. The initial orientations for the discs were the same as in NB03, Table 1. The merger remnants were allowed to settle into dynamical equilibrium for approximately 10 dynamical timescales after the merger was complete. Then their equilibrium state was analyzed.

The total sample comprises of 96 merger remnants of which half of them were run with a gaseous component. We adopt the following nomenclature for the mergers presented: The first two numbers give the mass ratio of the progenitor discs, i.e. 11 or 31. The letter 'C' stands for analysing a collisionless merger (disc and bulge particles), 'S' stands for analysing only the stellar component of a gaseous merger (disc and bulge particles) and 'GS' analysing the total luminous part of a gaseous merger (disc, bulge and gas particles). The last number denotes the merging symmetry. For example, the abbreviation 11C5 means: a collisionless equal mass merger with merging symmetry 5. The mergers we have analysed in detail, a comment regarding their kinematic peculiarity and the detailed orbit parameters of the merger they resulted from, can be found in Table 1.

3 2-DIMENSIONAL DATA ANALYSIS

3.1 LOSVDs

Every remnant was projected along the long axis (X-axis, YZ-projection), the intermediate axis (Y-axis, XZ-projection) and short axis (Z-axis, XY-projection) of the moment of inertia tensor defined by the 40% most tightly bound stellar particles. For the 2D analysis we binned particles within the central 3 length units on a grid of 48×48 cells. This corresponds typically to 2-3 effective radii depending on projection (see ? for the exact determination of r_e). To include seeing effects we created for every luminous particle 10×10 pseudo-particles with identical velocities on a regular grid with a total size of 0.125 unit lengths centered on the original particle position. The mass of the original particle was then distributed to the pseudo-particles weighted by a Gaussian with a standard deviation of 0.1625 unit lengths. Thereafter the pseudo-particles were binned on a 48×48 grid.

For the kinematic analysis we binned (mass weighted) all pseudo-particles falling within each grid cell in velocity along the line-of-sight. The width of the velocity bins was set to a value of 0.1 for line-of-sight velocities v_{los} in the range $-4 \leq v_{\text{los}} \leq 4$. This resulted in 80 velocity bins over the whole velocity interval. Using the binned velocity data we constructed line-of-sight velocity profiles (LOSVD) for each bin of the 2D grid. Subsequently we parameterized deviations from the Gaussian shape of the velocity profile using Gauss-Hermite basis functions (??). The kinematic parameters of each profile (σ_{fit} , v_{fit} , H_3 , H_4) were then determined simultaneously by least squares fitting (??).

3.2 Kinometry

Surface brightness and line-of-sight velocity are both moments of the stellar distribution function. The surface brightness is its zeroth-order and the line-of-sight velocity the first-order moment. However, there is a fundamental difference between the 2D fields of both moments: as the surface brightness is an even moment its iso-contours are point-symmetric (and therefore closed) and as the line-of-sight-velocity is an odd moment its iso-contours are point-*anti*-symmetric and therefore open. While isophotal shapes were found to be very close to perfect ellipses, such a choice is not obvious for iso-velocity contours. K06 found empirically that the kinematics of early-type galaxies resemble very closely those of inclined discs, which in many cases can be well described by circular motion. If you would project a circular orbit which moves in the plane of the galaxy on the sky, then it would follow a simple cosine law:

$$V(R, \psi) = V_0 + V_C(R) \sin i \cos \psi, \quad (1)$$

where R is the semi-major axis length of the projected circle on the sky, V_0 the systemic velocity, V_C is the ring circular velocity, i is the ring inclination and ψ is the azimuthal angle measured from the major axis of the ellipse (their Eq. 5).

However, as the authors state, elliptical galaxies are spheroids and not inclined discs and therefore their assumptions will be violated in nature. The next step is to see how far galaxies deviate from the simple cosine law. This can be achieved by the means of a Fourier series. A map of a moment of the LOSVD can be generalized to

$$K(a, \psi) = A_0(a) + \sum_{n=1}^N A_n(a) \sin(n\psi) + B_n(a) \cos(n\psi), \quad (2)$$

where ψ is the eccentric anomaly and a the semi-major axis of the ellipse (their Eq. 6). K06 find that only few terms are needed (up to third order) to find a good description of the 2D data.

In the case of an even moment the fitting procedure is similar to what is done in conventional photometry, while in case of an odd moment their algorithm tries to minimize all terms of the harmonic expansion except $B_1(a) \cos(\psi)$, which according to their Ansatz carries the major contribution to the map of an odd moment of the LOSVD. In the first stage of the fit, these terms are minimized on a grid of position angles (Γ) and flattenings ($q = 1 - \epsilon$). After the ellipse, which describes the velocity profile best, has been found, the rotation curve is extracted again and Fourier-analysed to arbitrary order.

We follow the authors in using the following four parameters to quantitatively describe kinematic 2D maps: The already mentioned Γ , which measures the alignment of the rotation and q which can be interpreted as the opening angle of the iso-velocity contours. They argue that although the amplitudes of the separate cosine and sine terms in principle describe different properties of the maps, it is better for systems which are not axisymmetric to collect the amplitudes of sine and cosine terms of the same order (their Eq. 10):

$$k_n = \sqrt{A_n^2 + B_n^2}. \quad (3)$$

For $n=1$ we get the term k_1 , which represents the amount of line-of-sight bulk rotation in case of a velocity map. The authors found that the ratio k_5/k_1 , where k_5 is the first higher-order term of the expansion which has not been fitted to the map and expresses the deviations from regular rotation, is sensitive to the presence of multiple kinematic components in a galaxy.

For a detailed description of their analysis method we refer the reader to the original paper K06.

4 RESULTS

In this section typical examples for 2D surface density, velocity and velocity dispersion maps of individual merger remnants are shown. We highlight the most important kinematic features and quantitatively analyze them. We will use the results of our previous study on the orbital structure of merger remnants (?, henceforth JNB05) to interpret our findings for all the maps presented in this paper. The apparent long axis of the remnants will be horizontally oriented for all the maps presented in this paper. In general we show maps for the collisionless stellar particles (C), the stars of the simulations with gas (S) and the stars in combination with gas (GS), as an indication of what the star would look like in the case of late star formation. However, during the merger a significant fraction of the gas falls to the center (see NJB06) and overpowers the signal in the central bins. In this case a reliable analysis for the center of the remnants is not possible. All maps are shown in the original SAURON colour scheme as devised by Cappellari & Emsellem (2001) and included in the Kinometry distribution.

4.1 Surface Density Maps

It has been shown by a number of investigations that the presence of gas during a merger event makes the remnant more axisymmetric (?). NJB06 have shown that this effect is stronger for 1:1 remnants which are intrinsically more triaxial (or prolate) than 3:1 remnants. Fig. 1 shows this effect for the 2D stellar surface density distribution of a collisionless 1:1 remnant and its counterpart, simulated with gas. Just by eye it is obvious that this particular remnant becomes much rounder if gas is included. Its intrinsic b/a changes from 0.83 to 0.95, while c/a increases even more significantly from 0.51 to 0.81. This is one of the few remnants in which the major axis tube fraction increases compared to the collisionless case from 5% to 11%. Next to minor axis tubes, also outer major axis tubes support potentials of spherical shape. So an increase of this fraction is to be expected (for a detailed description of orbit classification in merger remnants

see JNB05). The effect of gas on the surface density maps of 3:1 remnants is in general hardly detectable (see Fig. 2) as the collisionless remnant is already rather axisymmetric.

4.2 Rotation of Collisionless Remnants

In Fig. 3 we show the line-of-sight-velocity field of two collisionless 1:1 remnants and one collisionless 3:1 remnant 31C6 with regular rotation. The properties of 3:1 remnants do not change significantly with the initial disc orientations of the progenitors (see Fig. A6). Therefore this example is typical for this mass ratio. The remnant 11C3 shows also regular rotation, despite of being an equal-mass merger, albeit with a lower amplitude than 31C6. 11C3 is the 1:1 remnant with the highest minor axis tube fraction, but it is rather an exception, as in general the rotational structure of equal-mass merger remnants is more complicated and depends on the initial disc geometry (see Fig. A1). In the most extreme case a 1:1 merger remnant can exhibit almost no rotation within in an effective radius, like 11C5, which has the highest box orbit fraction of all merger remnants. All remnants in Fig. 3 show no rotation for face on projections, giving no indication of their true intrinsic orbital structure.

Turning to a kinematic analysis, we must note that the 2D velocity maps of 1:1 mergers are sometimes too complex to be fitted adequately with ellipses. Very low rotation causes the ellipse fitting algorithm to extract erratically changing position angles with radius. We therefore restrict the full parameter space for Γ , which can normally vary between 90° and -90° , to values between $\pm 2^\circ$, as we know that we look at edge-on projections, aligned with the x-axis. Note that this could represent a serious problem for observers who are not in the fortunate situation to know the 3-dimensional structure of the galaxy they investigate. However, we still allow the q parameter to vary freely. This procedure does not work, if the 2D velocity map shows strong kinematic misalignment, as the extraction along the wrong position angle will miss most of the rotation. In this section, we therefore focus only on aligned 1:1 remnants. Fortunately the 3:1 remnants have almost no kinematic misalignment.

As indicated before, 11C3 and 31C6 show a rising bulk rotation k_1 curve (Fig. 4), while 11C5 has almost no amplitude at all in the center. In the same Figure, right side, we plot the k_5/k_1 ratio. In the center of 11C5 we find a k_5 coefficient as large as the k_1 coefficient, while the other remnants have values closer to what is observed in the galaxies (see Fig. 7 of K06). The extremely large value of k_5 is caused by the box-orbit population, which is dominant in the center and gets smaller at larger radii, where minor axis tubes are more populous. We test this by artificially removing the particles classified as box orbits, and analysing the 2D velocity field of the remaining particles. The most dominant orbit class is now the minor axis tube and the amount of rotation increases while at the same time the ratio k_5/k_1 decreases significantly.

4.3 Kinematic Twists and Misalignment

A galaxy is kinematically misaligned if its rotation axis is not aligned with its photometric major axis. In the top row of Fig. 5 we show an example of a collisionless remnant with

misaligned rotation, which is caused by a large fraction of major axis tubes. 11C12 shows the strongest rotation in the XZ projection (major and minor axis tubes are seen), relatively little rotation in the YZ projection (only minor axis tubes are visible) and considerable minor axis rotation in the XY projection (only major axis tubes). Interestingly, if re-simulated with gas, the stellar remnant shows a similar kinematic structure, however, the fraction of major axis tubes decreased from 24% to 12% and the fraction of minor axis tubes increases from 21% to 61%. They disproportionately gain because also the number of particles moving on box orbits decreases. This evolution is visible in the second row of Fig. 5. The YZ projection of stellar component of the remnant with gas shows more rotation. Also the minor axis rotation in the XY projection (bottom right in Fig. 5) is reduced, which can only originate from major axis tubes.

Because of the strong kinematic misalignment the assumption of a constant position angle is of course wrong. To solve this problem we follow the alternative procedure, proposed by K06, and extract the rotation curve by averaging over circles (see Appendix A of K06). Despite this simplification the authors point out that k_1 and k_5/k_1 are still useful indicators for the bulk motion and deviations from regular motion. But because a circle has no defined position angle, we have to recover the phase angle

$$\phi_1 = \arctan \left(\frac{A_1}{B_1} \right), \quad (4)$$

where the phase angle ϕ_1 represents the direction of the bulk rotation (their Eq. 10).

By convention of the so called North of East system 90° and 270° represent iso-velocity contours which are aligned with the major photometric axis, but rotate in opposite directions. As shown in Fig. 6 the collisionless remnant is at the center almost maximally misaligned with a $\phi_1 = 180^\circ$ and slowly changes to about $\phi_1 = 220^\circ$ at larger radii, i.e. the remnant has a kinematic twist (KT). This reflects the fact that the fraction of minor axis tubes increases with increasing radius, which skews the rotation more towards the major photometric axis. Nearly the same happens for the gaseous remnant, only that the strongly misaligned region is smaller, as minor axis tubes are already populated at smaller radii. The KT is now stronger between an outer disc-like component and a the remnant population of major axis tubes in the center.

4.4 The Flattening of Iso-Velocity Contours

K06 argued with the example of four early-type galaxies taken from the SAURON sample that different kinematic flattenings, q , show to what extent a galaxy is an axisymmetric rotator, in which case q remains constant with radius (see their Fig. 7). Two of their galaxies show peculiar flattenings, one with a radially rising q and one with very wide opening angles in the center (NGC 2549), but dropping to $q = 0.4$ at larger radii.

As the q profile of NGC 2549 reminds us of flattenings found in 3:1 remnants, we will study in this section the influence of gas on the q -parameter in our 3:1 merger remnants. Their kinematics are much simpler than in 1:1 remnants, because it is much more difficult to populate major axis tube orbits in a 3:1 merger remnant and hence their kine-

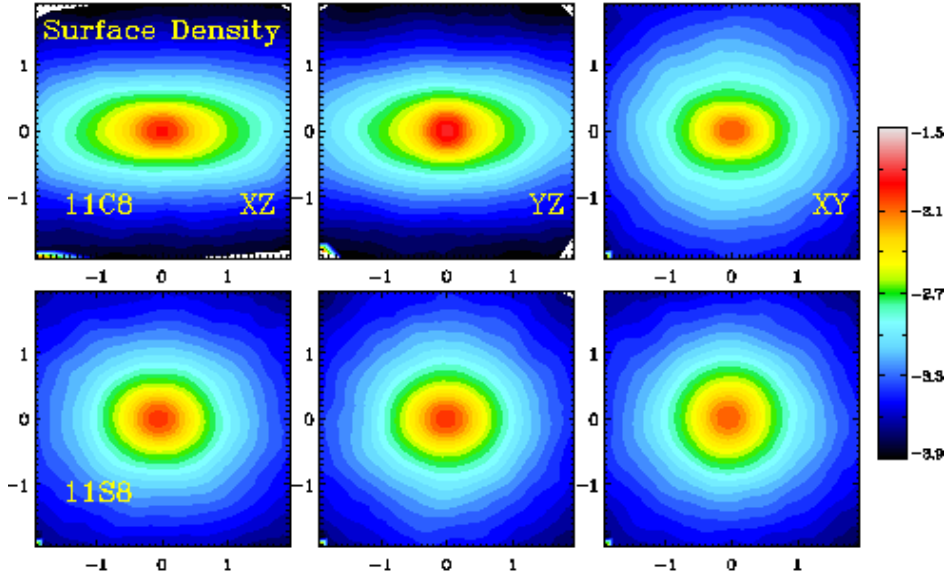


Figure 1. 2D surface density maps for the equal mass remnant with geometry 8. The projections along the three principal axes for the collisionless remnant (11C8, top row) are compared to the stellar component of the corresponding remnant with gas (11S8, bottom row). 11C8 is clearly triaxial whereas 11S8 is nearly round due to the influence of the additional gas component on the distribution of stars. One unit of lengths corresponds to roughly one effective radius (?)

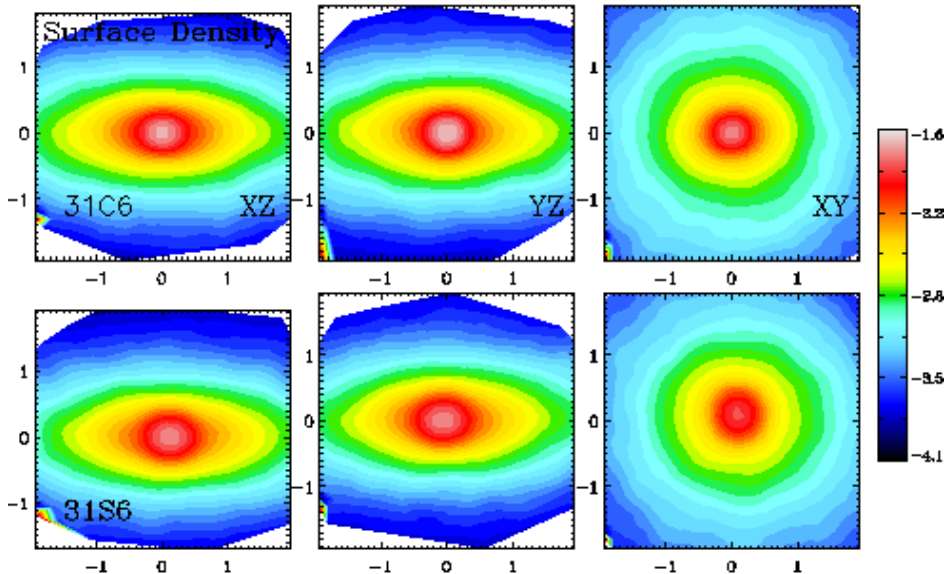


Figure 2. Same as Fig. 1 for the 3:1 merger with geometry 6. There is no obvious influence of gas on the stellar distribution.

matic twists are almost negligible. Also, all of them show significant rotation in most of the projections, which is a precondition to apply the kinematical analysis. We analyze the YZ and the XZ projection, i.e. edge on projections, of every remnant. To get an overview of how the q -parameter changes with projection and with the inclusion of gas, we calculate the mean q for every radial bin and compare four subsamples: 3:1 collisionless YZ and XZ-projection and 3:1 dissipational mergers YZ and XZ-projection. We can see in Fig. 7 that the iso-velocity contours of the XZ-projection of

the collisionless remnants have in general a smaller opening angle in the outer regions than for the YZ-projection, reflecting the more extended, boxy shape of the minor axis tubes for the YZ projection (NJB06). The stellar remnants whose progenitors had a gaseous component, are almost axisymmetric and therefore the flattenings are not very different between the two projections. It is, however, evident from the plot that the q of the stars in the gaseous remnants is significantly lowered at radii smaller than two effective radii. Interestingly for large radii we find slightly larger

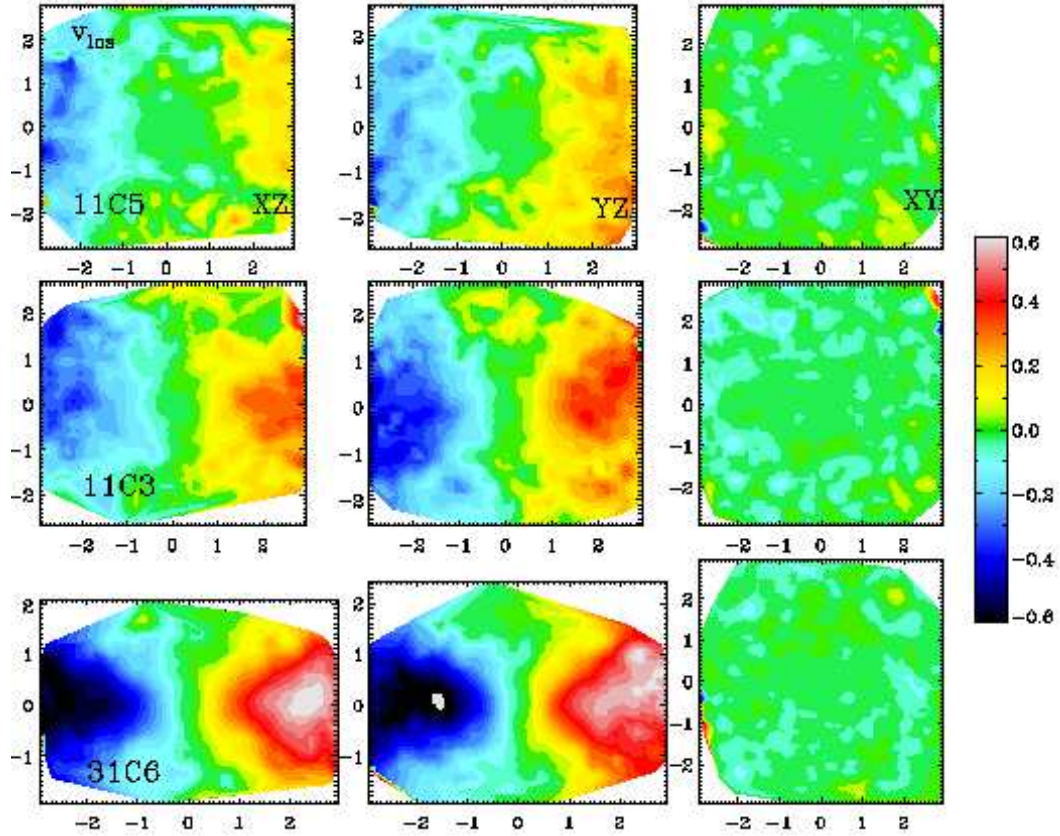


Figure 3. Two dimensional line-of-sight velocity field for the collisionless 1:1 remnant 11C5 (top row), the 1:1 remnant 11C3 (middle row) and the 3:1 remnant 31C6 (bottom row). The remnant 11C5 shows very little rotation, even for the edge-on projections. The other two remnants show regular rotation in the edge-on projections and no rotation in the face-on projection.

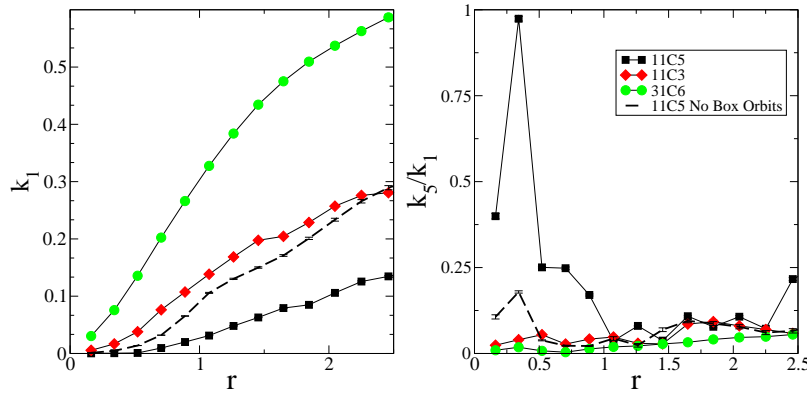


Figure 4. *Left:* Bulk rotation (k_1) for three collisionless remnants for the XZ-projection. The remnant 11C5 shows almost no rotation in the center. *Right:* The k_5/k_1 ratio is very large in the center of 11C5. This is caused by the strong box orbit population, as shown by the k_5/k_1 curve with the box orbits removed. The remnant 31C6 has the lowest values which is a signature of very regular rotation.

opening angles in the gaseous remnants as compared to the XZ-projection of the collisionless remnant. This is probably because at large radii the surviving part of the progenitor disc dominates the rotation and the flattening of the initial disc is very low as indicated in Fig. 7 (blue line).

4.5 Counter-Rotating Cores

It has been shown by ? that equal-mass mergers can result in the formation of kinematically decoupled components (KDCs). ? points out that retrograde encounters naturally lead to counter-rotating subsystems in the gaseous component of merger remnants, but for some merging symmetries the central subsystems might disappear easily when the im-

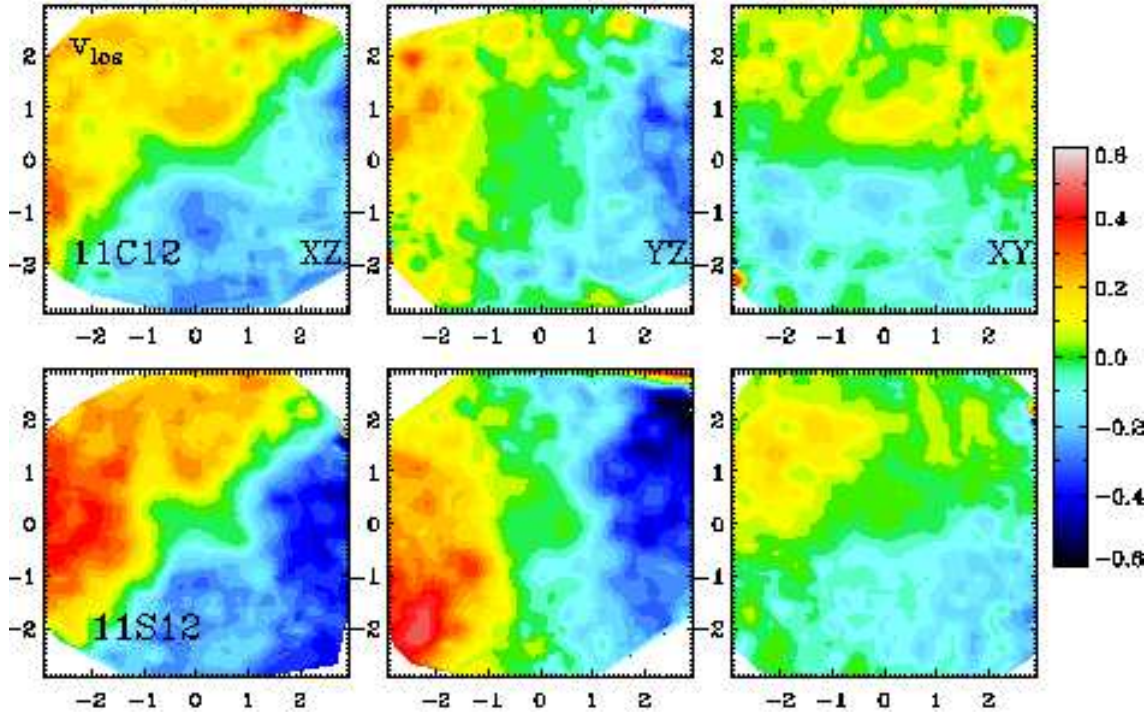


Figure 5. The 1:1 remnant with geometry 12 is strongly kinematically misaligned and shows strong rotation around its Long Axis. Even the presence of gas does not completely wipe out this kinematic structure. The amplitude of rotation is lower in the collisionless remnant (top row).

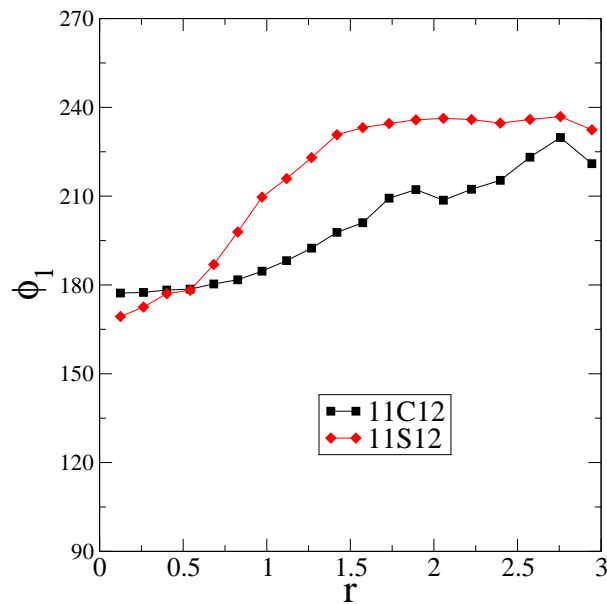


Figure 6. The kinematic phase angle ϕ_1 of the stellar rotation for two equal mass merger remnants which originated from the same initial conditions, but one with gas (11S12) and one without gas (11C12). The collisionless remnant shows stronger kinematic misalignment, while the stronger minor axis tube population in the gaseous remnant leads to a stronger kinematic twist.

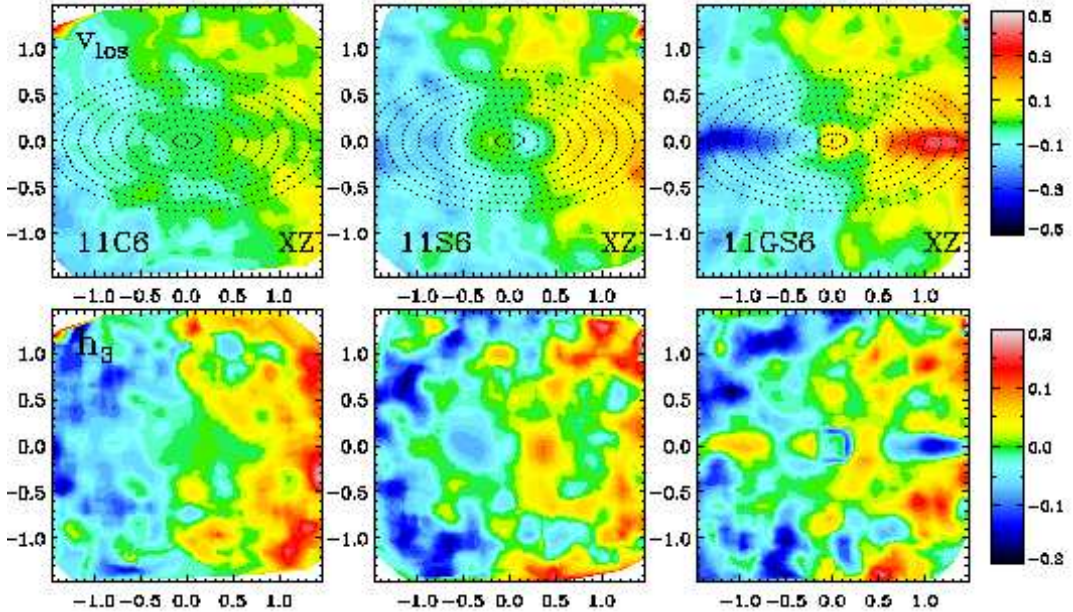


Figure 8. Top row: Projected 2D line-of-sight velocity in the XZ projection for the collisionless remnant (11C6), the stellar remnant of the counterpart with gas (11S6) and including the gas (11GS6) component assuming that all gas turned into stars after the merger was complete (from left to right). In the middle panel a counter-rotating stellar core (CRC) is clearly visible. In the right panel the kinematic signature of the thin disc appears. The ellipses, which have a $q = 0.5$ and $\Gamma = 0^\circ$, along which we extracted the rotation curves are overplotted. Bottom row: Two dimensional distribution of h_3 for the same remnants. There are strong signatures for the counter-rotating core and the thin disc (middle and right panel).

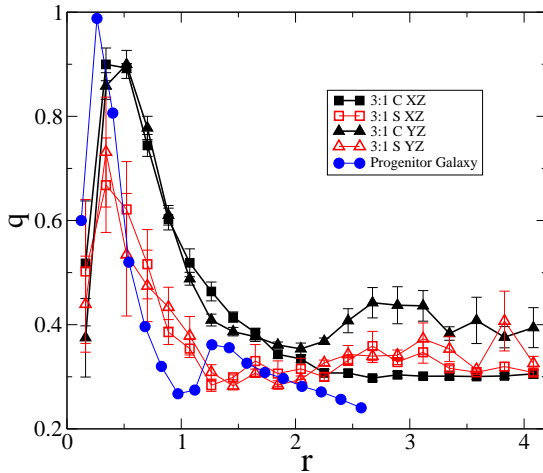


Figure 7. Flattening, q , of the iso-velocity contours vs radius. The q parameter has been averaged at each radial bin for all 3:1 remnants for four cases: 3:1 collisionless merger XZ and YZ projection and 3:1 gaseous merger XZ and YZ-projection. Error bars indicate the rms at each bin. For comparison we plot the kinematic fit of a progenitor disc galaxy

pact parameter is changed. The exact reason remains elusive. We find counter-rotation in the gaseous component in about 50% of the 1:1 remnants and in only 1 out of 32 3:1 remnants. In contrast, in only one of the collisionless 1:1 mergers (11C16) a counter-rotating dynamical component is visible, which extends almost to one effective radius. Interestingly, the addition of gas induces the formation of

Counter-Rotating Cores (CRCs) in the 'old' stellar component of the merger remnant of which 11S6 is one of the best examples (see Fig. 8).

This can be more clearly demonstrated by a kinematic analysis, where we use fixed values for $\Gamma = 0$ and $q = 0.5$ to extract the rotation curve, which results in the smallest ratio k_5/k_1 and hence represents the CRC most accurately. We determine the rotation curve for all three cases (collisionless, only the stellar component of the remnant with gas, gas and stars of the gas remnant).

K06 have presented a very instructive set of two-component test models in which they vary the alignment of the central component from aligned ($\Delta\Gamma = 0^\circ$) to counter-rotating ($\Delta\Gamma = 180^\circ$). In their Fig. 2 it is very well visible that the transition from the CRC to the bulk system is marked by a drop in k_1 and a peak in k_5/k_1 . Indeed on the left side of Fig. 9 we see a very similar behaviour of the k_1 coefficient for the system 11S6 which is the stellar component of the gaseous remnant. It initially rises and drops almost to zero at a radius of $r = 0.4$, before it rises again. Similarly the kinematic position angle changes by $\Delta\Gamma = 175^\circ$ at the same radius where k_1 drops to zero and then stays constant (Fig. 9, right side). This demonstrates that the central component is almost exactly counter-rotating. Neither the collisionless remnant (11C6) nor the total baryonic system (gas and stars, 11GS6) show any apparent signature of a CRC. The gas mainly settles in an extended disc, which overpowers the signal of the counter-rotating material.

In the bottom row of Fig. 8 we show the corresponding two dimensional h_3 maps. For the collisionless remnant v_{los} is correlated with h_3 . The stellar remnant with gas (lower

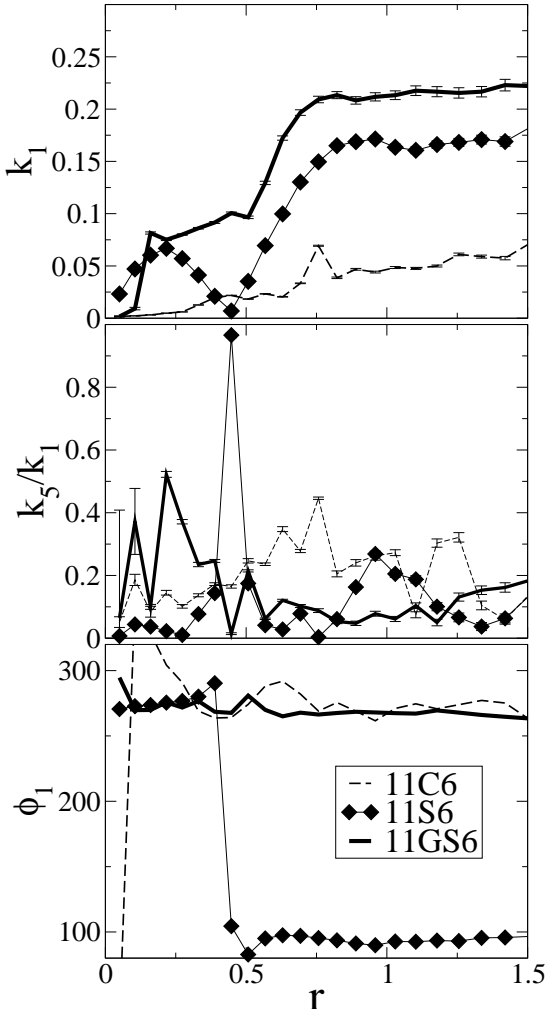


Figure 9. . Top: Rotation curves, k_1 , extracted along an ellipse with $q = 0.5$ and $\Gamma = 0^\circ$ centered on the photometric major axis. The curves are shown for the collisionless remnant (11C6), gas and stars of the dissipative remnant (11GS6) and the stellar component of the gaseous remnant (11S6), which has a Counter-Rotating Core (CRC). Middle: For 11S6, the ratio k_5/k_1 shows a strong peak at the transition radius between the CRC and the outer spheroid, as found in the test examples of K06. The other curves show no distinct features. Bottom: Reconstructed angular direction ϕ_1 of the rotation, k_1 . 11S6 shows a CRC with almost exactly 180° misalignment in its rotation (i.e. counter-rotation).

middle panel) shows the same correlation in the outer parts. In the region of the decoupled core, however, v_{los} is anti-correlated with h_3 . The gas disc (lower right panel) is clearly visible in the h_3 map of 11GS6 and shows an anti-correlation,

In the whole sample we can identify at least six stellar CRCs in dissipational equal mass merger remnants from the kinematic analysis (see Fig. A2).

4.6 The Influence of Gas on v_{los} and h_3

In Fig. 10 we show the 2D line-of-sight-velocity map of a 3:1 remnant and the corresponding distribution of h_3 . For the collisionless remnant (left panels) v_{los} and h_3 are correlated inside $0.5 r_e$ and anti-correlated in the outer parts. This be-

haviour is typical for collisionless 3:1 remnants (??; NJB06) and is not consistent with observations of elliptical galaxies (??). If gas is present during the merger the correlation at the center disappears even if only the stellar component is considered (middle panel), leading to an overall anti-correlation which is even stronger if we include the gas component in the analysis (right panels). The correlation of v and h_3 at the center can be explained by the presence of box orbits in most collisionless merger remnants. Firstly, they have a mean angular momentum of zero and therefore are preferably populated at small radii and secondly, as the orbits have no definite sense of rotation, they also have a skewness of zero, independent of the viewing angle (see also JNB05, Fig. 18 and Sec. 6). Gas is suppressing the population of box orbits, resulting in a more realistic skew of the velocity profiles of the merger remnants, which is discussed in detail in NJB06. The velocity field is also more peaked towards the center if a dissipative component is present in the merger.

4.7 Systems with Polar Rings

A particularly interesting 1:1 remnant is shown in Fig. 11. In this case the gas forms a large scale gas ring which is inclined by $\Gamma = 95^\circ$ with respect to the photometric major axis of the galaxy and a central gaseous disc. The kinematic analysis reveals the different amount of rotation in the gas and in the stars. As the gas ring is very narrow we extract the rotation curve along an ellipse with a $q = 0.3$ and with the same alignment, i.e. $\Gamma = 95^\circ$, as the ring. As apparent from the upper panel of Fig. 12 already in the collisionless remnant does a significant fraction of stars move on polar orbits. The gas also seems to have a higher line-of-sight bulk motion than the stellar component. The ratio of k_5/k_1 (Fig. 12, lower panel) is high for the gaseous component at the center of the remnant. At the radius of the polar ring itself, however, the k_5/k_1 ratio is lower indicating regular rotation.

The polar ring is the result of the initial conditions of this particular merger for which initially the discs of the progenitors are inclined to each other by nearly 90° . The properties of this remnant are similar to those of polar ring galaxies. ?? has shown that such systems can form in galaxy merging events. Our simulations differ insofar that both progenitor discs have gas and that we ran a larger sample of disc inclinations. Only in two out of 16 1:1 mergers was a significant amount of gas deposited in a polar ring. Typically this is just 10% of the initial gas mass or 1% of the total baryonic mass of the system. The gas in such a polar ring stems from one of the merging partners only. We do not find any significant polar ring structures in 3:1 mergers.

Observed polar ring galaxies, though, have a comparable amount of mass in the polar ring and in the central component, typically an S0 galaxy (see e.g. ??). Our simulations already start with too little gas (10% of the total mass) to form such a system. Alternatively, such systems can form by cold accretion (??) in a cosmological context.

4.8 Line-of-sight velocity dispersion

In Fig. 13 we show the 2D velocity dispersion maps of a 1:1 merger remnant and a 3:1 merger remnant for one edge-on projection (XZ projection). Both collisionless remnants

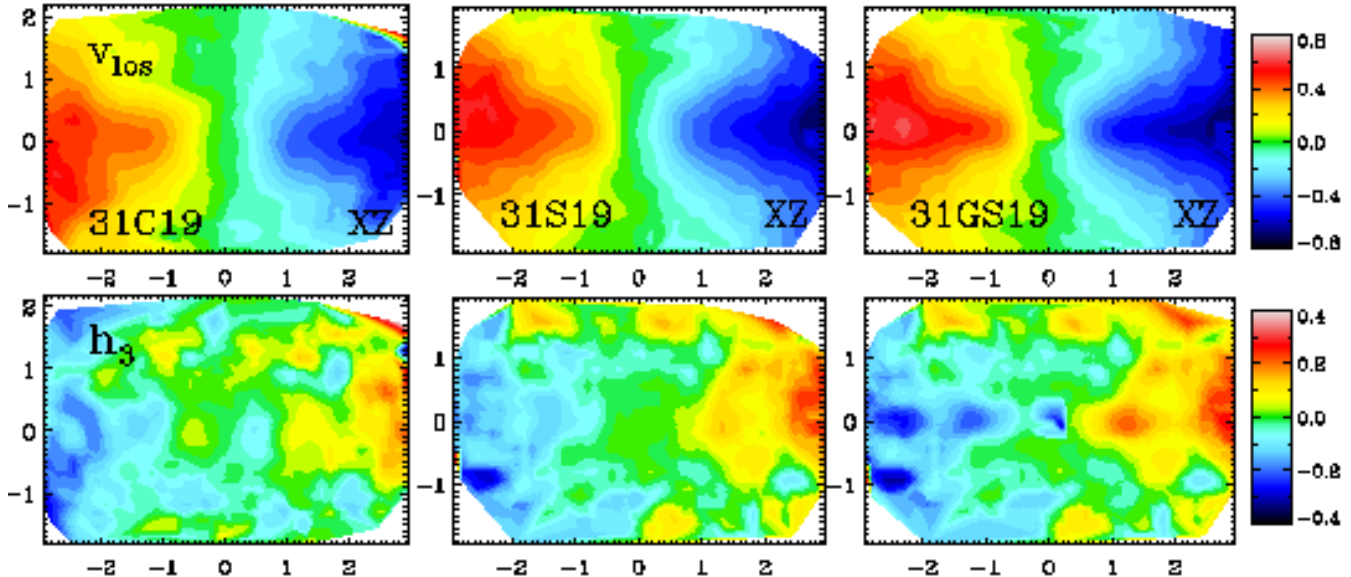


Figure 10. Same as Fig. 8 but for the 3:1 remnant with geometry 19. For the collisionless remnant (31C19) v_{los} and h_3 is correlated in the inner parts and anti-correlated in the outer parts (top and bottom left panel). Gas changes the stellar properties of the stars in the inner parts and now v_{los} and h_3 is weakly anti-correlated (top and bottom middle panel). If gas is included in the analysis a strong anti-correlation becomes visible (top and bottom right panels).

31C19 and 11C6 show a clear dip of the velocity dispersion at the center. This feature is a signature from the initial conditions. The bulge was setup with a γ density distribution whose velocity dispersion drops towards the center. However, the stellar dispersion of the remnant with gas shows a clear peak towards the center, again for both mass ratios 31S19 and 11S6. In this case the central gas concentration leads to adiabatic compression and heating of the stellar component at the center. The cold gas accumulated at the center becomes visible as we include the gas component in the analysis (right most plots in Fig. 13). Surprisingly the outer gas distribution shows different signatures for different remnants. An extended gas disc forms in the merger remnant 31GS19 which leads to a lower projected velocity dispersion than the surrounding stars. In 11GS6 the gaseous disc component, however, shows an even higher velocity dispersion than the stars as can be also seen if we extract the leading coefficient of the Fourier fit k_0 which represents the bulk velocity dispersion of the 2D data (see Fig. 14).

We can detect a ring-like depression at about one effective radius in the stellar velocity dispersion of the remnants with gas. This feature is particularly strong in the remnant 11S2 (top row of Fig. 15). As this depression can be detected in all three projections we most likely have a shell of low dispersion stars. The depression in σ corresponds to a positive h_4 indicating a LOSVD that is more peaked than a Gaussian.

5 COMPARISON TO OBSERVATIONS

The results of the previous sections can be compared with the SAURON sample. As only the kinematic analysis of four SAURON galaxies (K06) is published, we can not do much

more than visually compare the maps. We follow, however, loosely the categories as laid out by K06, which include low-level rotators, galaxies with kinematic twists and galaxies with multiple components.

Low-Rotation: The kinematics of the remnant 11C5 (Fig. 4), shows (scaled) rotation of below 10 km/s inside one effective radius, which is extremely low-rotation. There are many galaxies in the SAURON sample that are not rotating outside a fast rotating central KDC, the so called slow rotators (?). We find three examples of galaxies with a rotation below 20 km/s: NGC 4374, NGC 4486 and NGC 5846. All these objects are round and have elliptical or slightly boxy isophotes. Their high central velocity dispersion indicates that they are fairly massive and that a merger of two very massive late-type galaxies would be needed to destroy the rotation in the progenitors and increase the mass accordingly. The scenario of merging elliptical galaxies would be even more favourable, as already the progenitors would have very little rotation (?).

Kinematic Twists: A KT is indicated by a smooth change of the kinematic position angle. We find KTs only in 1:1 mergers which are violent enough to scatter stars from minor axis tubes onto major axis tube orbits. More than half of the 1:1 merger remnants show, at least at the center, iso-velocity contours twisting more than 30° . The frequency and amplitude in the simulated equal-mass merger remnants seems to be higher than for the KTs found in the SAURON sample. In contrast, 3:1 mergers do not produce any galaxy with a twist of more than 20° degrees, be it with or without gas. In this respect 3:1 mergers are in better agreement with observations.

Counter-Rotating Cores: We define CRCs as a subgroup of KDCs with a sudden kinematic twist of 180° . We find no CRCs in 3:1 remnants with or without gas and we find

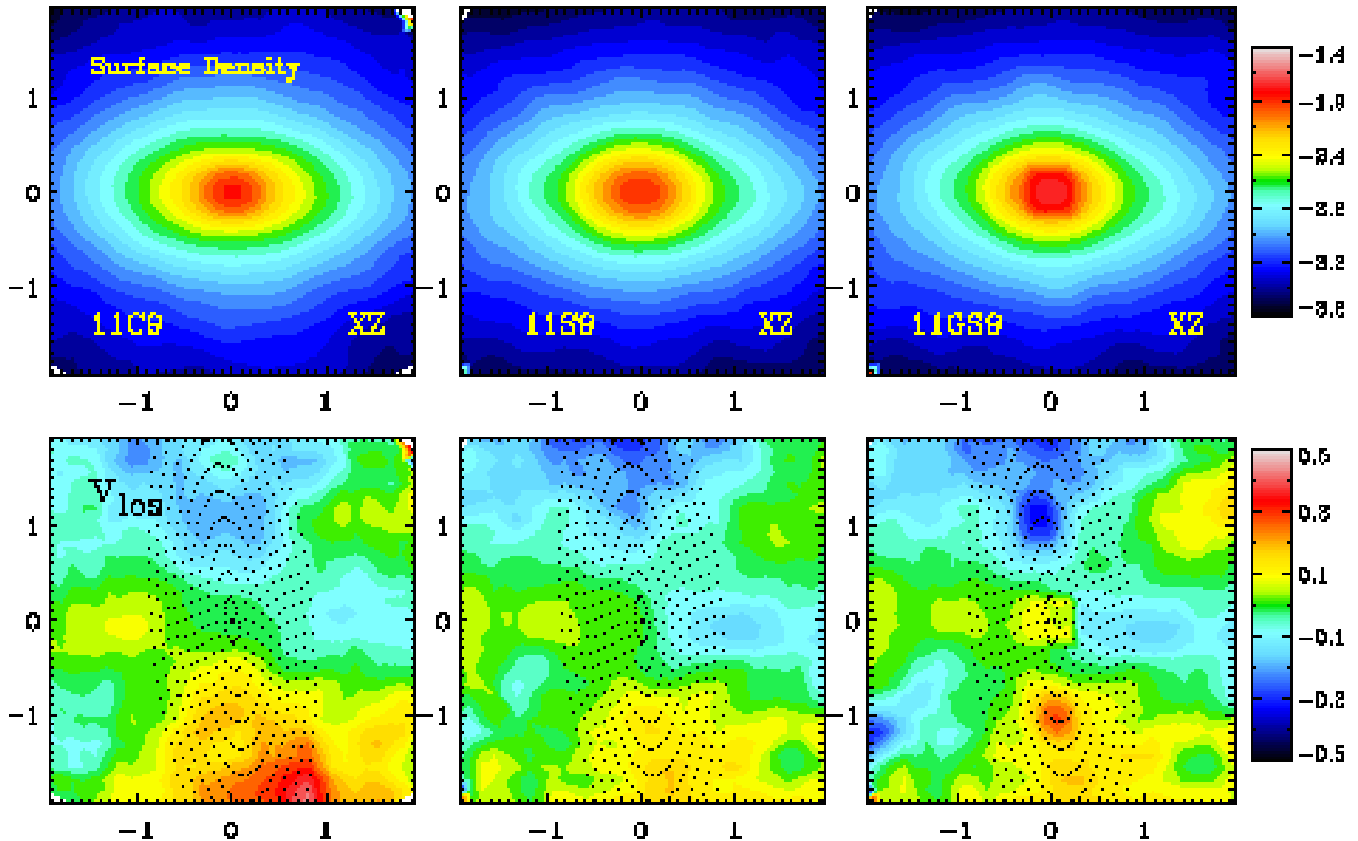


Figure 11. Top row: Surface density maps of the 1:1 remnant with geometry 9. The XZ projection is shown for the collisionless remnant 11C9, the stellar component (11S9) of the gaseous remnant and both, gas and stars (11GS9) of the gaseous remnant. Lower row: 2D Velocity fields of the same systems with the same projections. The ellipses, with $q = 0.3$ and $\Gamma = 95^\circ$, at which the rotation curve was extracted are overplotted. Gas settles in a large scale ring inclined by 95° with respect to the main stellar body. The signature is similar to polar ring galaxies. Very little mass lies in the polar gas ring itself which is therefore not visible in the surface density maps in the top row.

one candidate in a 1:1 collisionless remnant. For the stellar component of the 1:1 simulations with gas, we find at least six candidates for CRCs from the maps: 11S2, 11S4, 11S6, 11S13, 11S14 and 11S16 (see Figs. A2 and A5). In the SAURON data it appears that CRCs are common in so called low-rotators (but maybe CRCs stand out more, see ? for a discussion). Our findings are consistent with observations, because 1:1 mergers have in general much lower rotation than 3:1 merger remnants (NB03, NJB06). Our simulations imply that stellar CRCs in slow-rotators are formed in 1:1 mergers when gas is present. Interestingly, these CRCs formed from the old stellar population of the progenitor galaxies, together, possibly with stars formed during the merger itself (see ?). In 3:1 mergers fast rotating galaxies are formed without CRCs, in agreement with observations, although the OASIS observations show the presence of some small CRCs (?), which we would not have been able to resolve.

The $v - h_3$ Correlation: Collisionless simulations show that there is generally a positive correlation between these quantities in the center of the remnants (NJB06). The presence of gas would inhibit the population of box orbits, the orbit class responsible for positive correlations (see discus-

sion in Sec. 4.6). Contrary to what is seen in the collisionless remnants, we see no correlation of $v - h_3$ in the center of any galaxy in the SAURON sample. In the outer parts there are a few examples with positive correlations: NGC 1023, NGC 2699, NGC 4270 and particularly NGC 4526. This could be an indication for a presence of bars (?). This argues (see NJB06) against pure collisionless mergers as possible formation mechanism of rotating SAURON galaxies, in agreement with the discussion on CRCs, see above.

Opening Angle of Iso-Velocity Contours: In Sec. 4.4 we showed that on average 3:1 merger remnants with open iso-velocity contours have had less dissipation. This is because dissipation causes flat discs and an overall more flattened and axisymmetric potential. As more material now rotates in the equatorial plane, the iso-velocity contours are closing resulting in a smaller q . This result can not be easily compared in a statistical way to observations. Therefore we have chosen a pair of galaxies, which in the range of the SAURON observations have the same ellipticity ϵ and the same v/σ : these are NGC 7457 and NGC 4660, with $\epsilon = 0.44$ and $v/\sigma = 0.6$ (?). Although these galaxies appear in the v/σ - ϵ diagram at the same position, we find that the velocity maps of ? of these two galaxies look very different: the

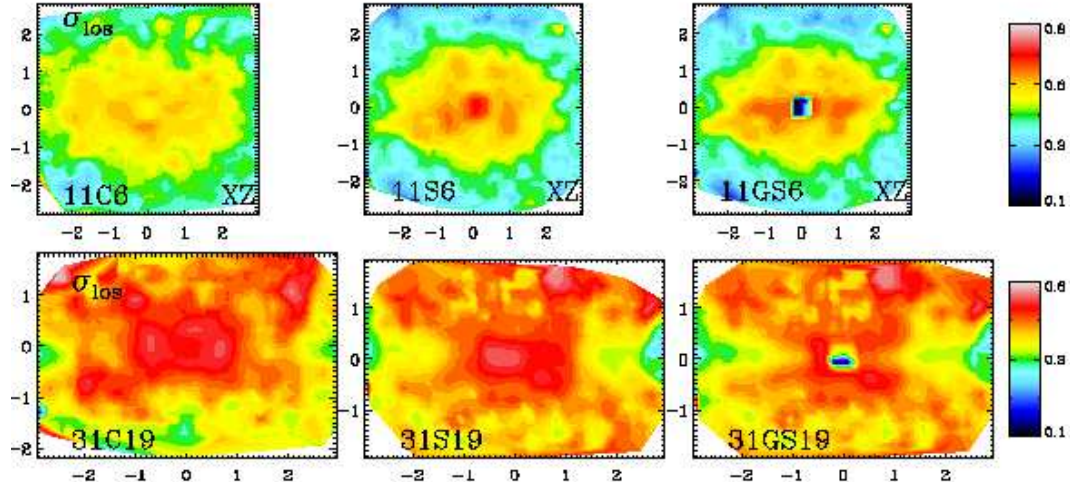


Figure 13. *Top row:* The velocity dispersion maps of the XZ projection for the 1:1 merger with symmetry 6. The velocity dispersion of the collisionless merger, 11C6, shows a depression of σ at the center. The dispersion field of the stellar component of the gaseous remnant, 11S6, however, is peaked, while the gas at the center, 11GS6, has a very low dispersion. A disc-like high dispersion strip is visible along the major axis (top right plot), if the gas particles are included in the analysis. *Bottom row:* A depression in the velocity dispersion is visible at large radii along the photometric major axis, both in the collisionless and in the stellar component of the remnant with gas. In the 31GS6 the gas settles partly into a cold stellar disc, which causes a V-shaped depression in the velocity dispersion even at small radii (see also Fig. 14)

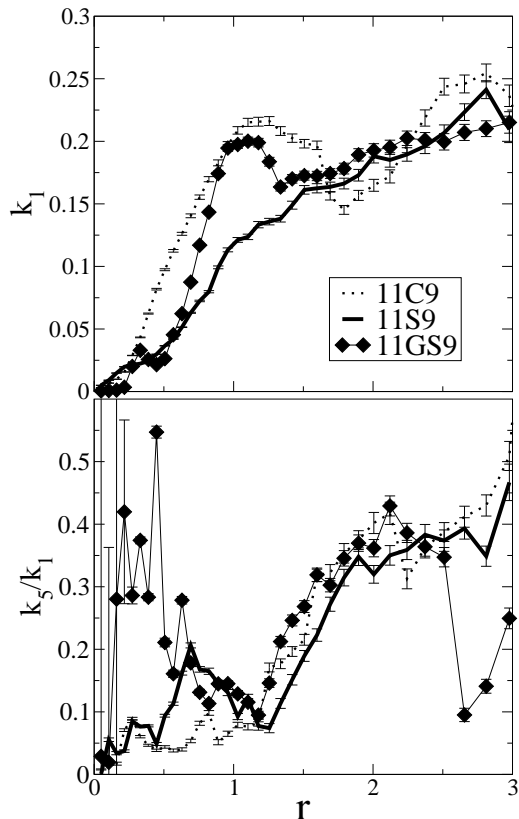


Figure 12. *Top:* Rotation curve, k_1 , extracted along ellipses with a $q = 0.3$ and a $\Gamma = 95^\circ$ centered on the polar gas ring (see Fig. 11). Rotational structure is already present in the collisionless remnant. The gas ring shows a higher rotation than the stellar component in the gaseous remnant. *Bottom:* k_5/k_1 ratio is lowest at the radial position of the ring.

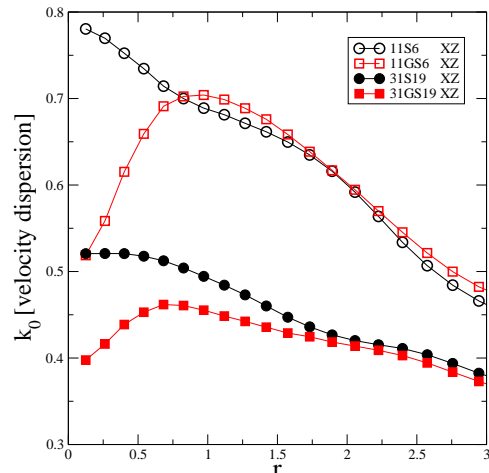


Figure 14. Dispersion profiles extracted from 2D velocity dispersion data for a 1:1 and a 3:1 gaseous merger, with and without the gas component included, for the same edge-on (XZ) projection. The profiles with the gas component show strong central depressions in σ . The outer gas component in the 1:1 remnant has even higher dispersion than the stellar component, while in the 3:1 remnant the opposite is the case (see also Fig. 13).

velocity contours in NGC 7457 are much more open than those for NGC 4660. This indicates that much more dissipation was present in the formation of NGC 4660, probably causing a flattened disc-like component in this galaxy. The ellipticity in the outer parts, from the RC3 (de Vaucouleurs, 1993), also is very different: 0.41 for NGC 7457 and only 0.21 for NGC 4660. This gives support for the presence of a second flattened component in the middle of NGC 4660. For NGC 7457 we can not infer its intrinsic flattening, but it is

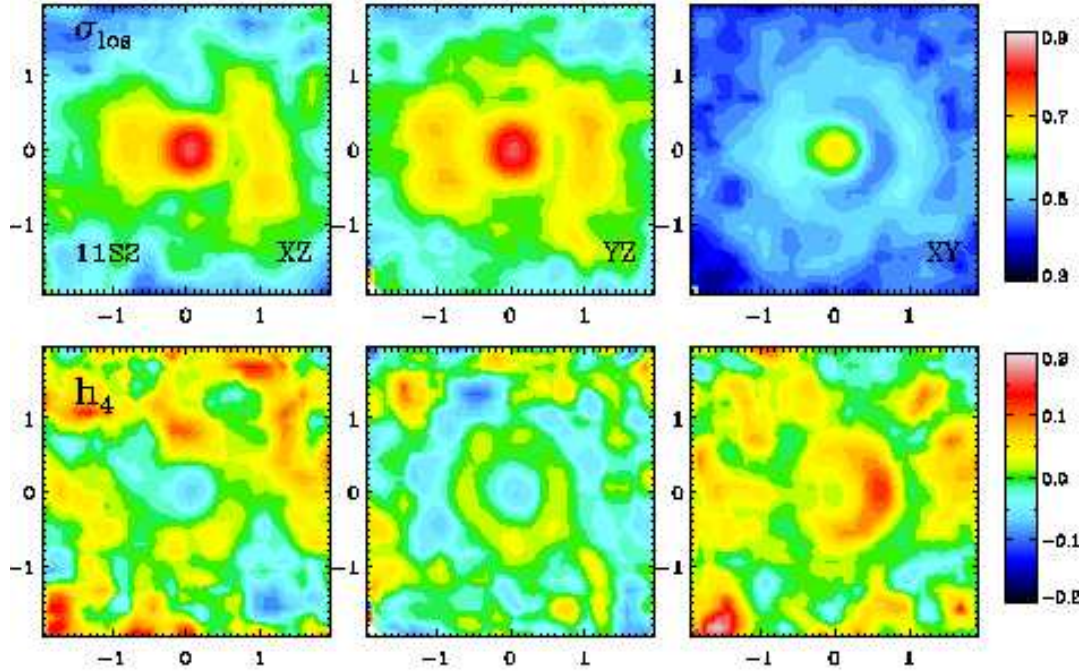


Figure 15. Projected 2D velocity dispersion for remnant 11S2 (top row) the the 2D distribution of h_4 for the same projections (bottom row). A depression of σ at about $0.5r_e$ is clearly visible. In the same region h_4 changes sign and becomes positive indicating a LOSVD more peaked than a Gaussian.

likely to be constant with radius, since the ellipticity profile is constant (?).

Polar Rings: As laid out in Sec. 4.5, we find one very pronounced polar ring in the merger 11GS9. This polar ring is present in simulations with or without gas. In the SAURON survey the only two examples of polar rings are NGC 2685 and NGC 2768. Both polar rings are only visible in the gas (?). The radial extent of the polar ring in the merger is very similar to what is found in these two observations. There appears to be a fundamental difference between simulations and observations, as no stellar polar ring is found in the data. The statistics, however, is very small, so no strong conclusions can be drawn here. There are observational cases known of stellar polar rings (e.g. NGC 4365 ?; ?), but these are generally small, not going as far out as one effective radius.

Low σ Rings: In some equal-mass merger remnants with gas we find ring-like depressions in σ for all main projections. Without gas we do not find them at all. Such a feature has been reported for one SAURON elliptical galaxy only: NGC 5813. In the spiral galaxy NGC 4314 (?) a similar situation is visible: a star formation ring with a low gas velocity dispersion and a high stellar dispersion. These features are too common in the mergers to be entirely realistic, but if they exist in galaxies they can be a strong indication for dissipation.

Central σ Drops: In almost all merger remnants which were formed from progenitors with a dissipational component, a significant fraction of the gas falls to the center, showing a very low σ_{los} in the maps. In contrast, the velocity dispersion of the stars is increasing towards the center.

In general the SAURON observations for early-type galaxies also show peaks in σ in the center, in agreement with the simulations. There are a few objects with a central minimum in the velocity dispersion: these are NGC 4382 and NGC 2768. For spiral galaxies, recently ? and ? found that dips in the central velocity dispersion are common, and that their frequency goes up with increasing Hubble type. They conclude that these dips are caused by central discs. In the case of the ellipticals the stars need about 1Gyr to dynamically heat up after formation (?). So we suspect that in these two galaxies the velocity dispersion dips are caused by young stars. For NGC 4382 this could be consistent with the line-strength maps measured by (?), but this idea does not work for NGC 2768 for which old populations are inferred in that paper. In this galaxy there must have been a different mechanism to keep the stars in the central region cold. This would be consistent with the center of some Sa galaxies, where velocity dispersion dips are found which are old (Peletier et al. in prep).

In general, collisionless remnants show bigger opening angles of the iso-velocity contours, more boxy isophotes, velocity dispersion profiles without central peaks, no strong anti-correlation between $v - h_3$. Remnants with a dissipational component show smaller opening angles of the iso-velocity contours for the same ellipticities (inclinations), strong dips in the gaseous velocity dispersion profile and an anti-correlation between $v - h_3$. Additionally CRCs are more common in equal-mass mergers than in mergers of unequal mass. We conclude that globally the non rotating subset of the representative SAURON sample of local galaxies agrees well with our 1:1 merger simulations, while the rotat-

ing subset can be reproduced by the dissipational 3:1 merger remnants.

6 SUMMARY AND CONCLUSIONS

We presented 2D maps of various moments of the LOSVDs of a large sample of 1:1 and 3:1 disc merger remnants with and without gas. Every remnant was resimulated with a dissipational component containing 10% of the luminous mass, allowing us to assess the influence of gas on the 2D fields. Additionally we performed a kinematic analysis using the method devised by K06 to quantify properties such as kinematic position angle or deviations from regular rotation.

The difference between equal-mass and an unequal-mass merger remnants is not only seen in photometric and global kinematic properties (?), but also in the 2D kinematics, which exhibits very different features. 1:1 mergers can lead to a merger remnant with low rotation. Also, orbit classes rotating around the major axis of the remnant can only be populated in significant numbers in 1:1 mergers, leading to kinematic twists, while 3:1 remnants rotate much faster and have almost no kinematic twists. All rotating collisionless mergers fail to reproduce the observed $v - h_3$ anti-correlation, because the population of box orbits in the center is not inhibited (NJB06).

The presence of a dissipative component of only 10% of the luminous disc mass in the progenitors can lead to a considerable change in the properties of 1:1 remnants. They are more round, kinematic misalignment is reduced, counter-rotating cores are forming and kinematic twist are more pronounced. Rare but observed features like polar gas rings form also in equal mass mergers. The effect of gas on 3:1 remnants is less dramatic. KTs, CRCs and polar rings are not formed or at least must be very rare. A noticeable change is that the opening angles of the iso-velocity contours become smaller. As shown in NJB06, the $v - h_3$ anti-correlation is now much better reproduced, especially if the gas component is included in the analysis.

Merger remnants show a variety of velocity dispersion features. Significant central velocity dispersion dips are caused by infalling gas. The central star component in the gaseous runs, however, is heated. Edge on gas discs can both exhibit lower velocity dispersion (as found in a 3:1 remnant) or higher velocity dispersion (as found in a 1:1 remnant) that the stellar component. Gaseous shell-like structures can imprint a ring-like depression in σ even on the stellar component, which is also visible in h_4 .

2D analysis of LOSVDs of N-Body simulations of galaxy formation are an additional tool to connect the formation history of galaxies with their observable kinematic fine structure. We defer a full statistical analysis to future work, with a larger sample of galaxies mergers, which will also take star formation into account.

The simulations and analysis presented here are a step forward in understanding the possible formation of ellipticals by mergers of discs. We focus on the influence of a small dissipative component, which is important to understand its impact on the dynamical properties of the remnants. However, additional physical processes like star-formation and feedback will change the detailed properties especially at the center of the remnants (??) and definitely have to be

considered for simulations with higher gas fractions (??). We believe that the global effects of dissipation even with star formation will be very similar to the results presented here. However, larger gas fractions might result in more massive stellar discs in the remnant. From a kinematic point of view disc merger remnants appear very similar to observed ellipticals, although questions regarding the age and metallicity of the stellar populations have to be addressed in the future. Analytical models of disc formation (?) as well as semi-analytical modeling (?) in combination with merger simulations (?) can be used to place further constraints on the disc merger hypothesis.

ACKNOWLEDGMENTS

We are grateful to Davor Krajnović for kindly providing and helping with the implementation of the Kinemetry software. The authors want to thank Karl Gebhardt for many helpful discussions and suggestions.

APPENDIX A: 2D VELOCITY MAPS AND KINEMETRIC DATA OF MERGER REMNANTS

This is a selection of 2D velocity maps of all the remnants. We have to restrict ourselves to the XZ projection, which is best suited for a kinematic analysis, as it shows the highest rotational amplitude. For the equal-mass mergers we analyze the maps by extracting the rotation curve along circles, as the kinematic twists are too strong. Although we do not study projection effects, we can see the merger to merger variance of the kinematic parameters, such as the kinematic misalignment in 1:1 mergers. A full list of the orbital parameters for all merging geometries is given in Tab. A1.

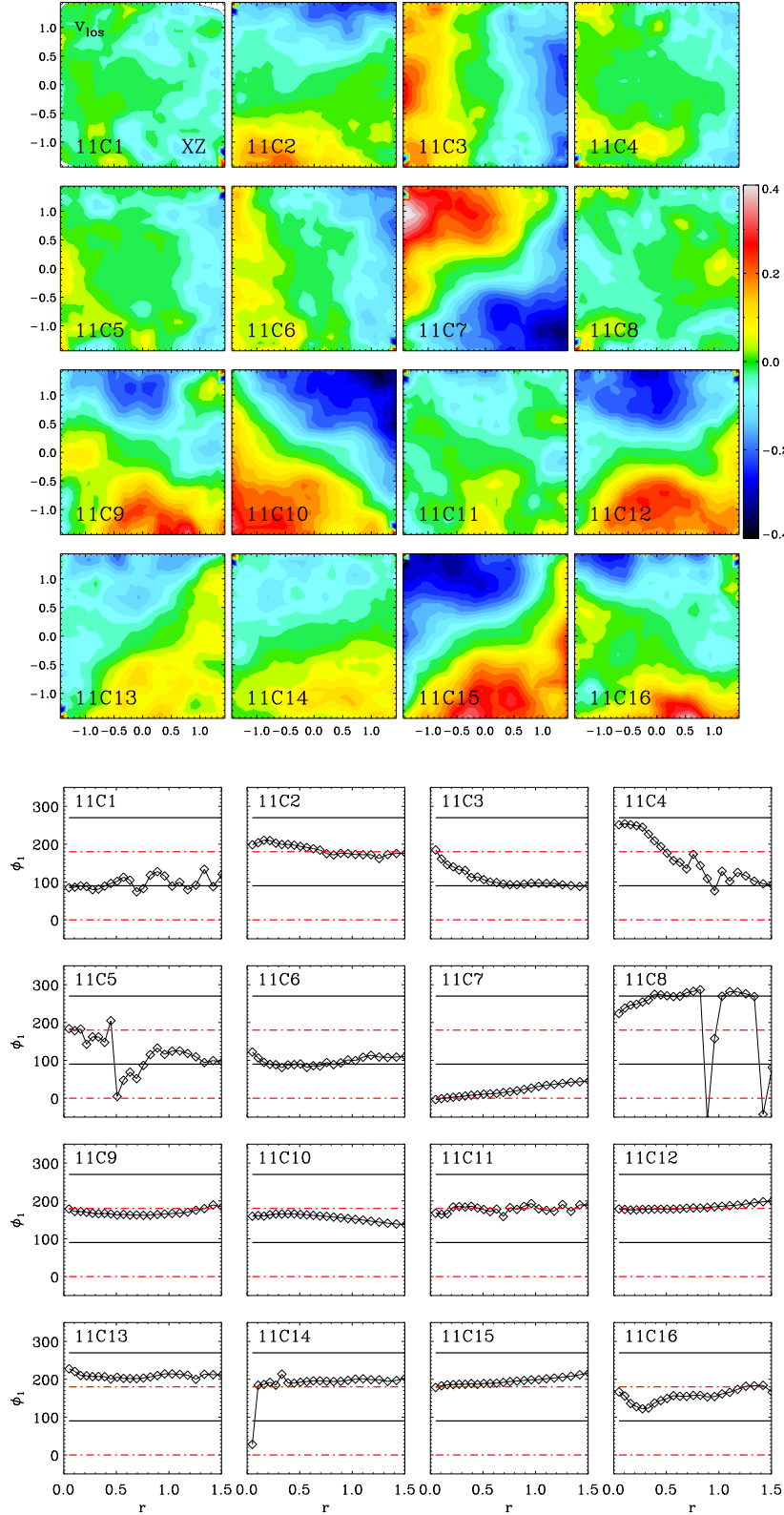


Figure A1. *Top:* Velocity maps for the collisionless 1:1 remnants for the XZ projection. *Bottom:* Corresponding kinematic position angles extracted along circles. By definition kinematic PAs of 90° and 270° signify rotation which is aligned with the photometric major axis (indicated by straight black lines), correspondingly 0° and 180° indicate maximally misaligned rotation (red dot-dashed lines). Strong kinematic misalignment is present in almost all remnants.

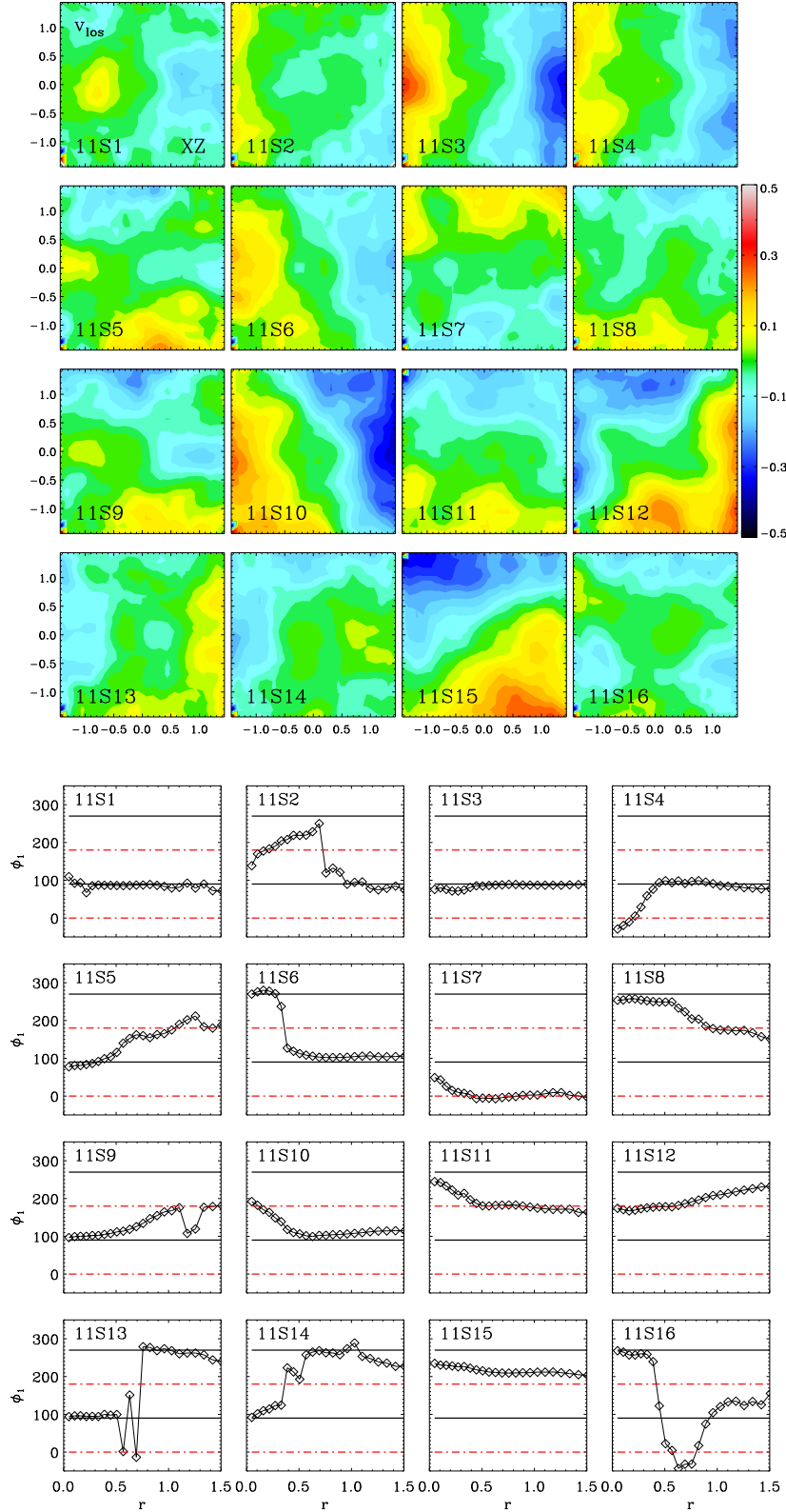


Figure A2. *Top:* Velocity maps for the stellar component of the 1:1 remnants which had progenitors with a gas component. *Bottom:* Corresponding kinematic position angles. Definition for horizontal lines as before. Sudden kinematic twists give indications for kinematic decoupled components in the center of the remnants. In the outer parts the remnants are more aligned than their collisionless counterparts (see Fig. A1)

Table A1. Full List of merging geometries. For unequal-mass mergers the first number indicates the orientation of the more massive galaxy as i_1 and ω_1 , the second number indicates the orientation of the more massive galaxy as i_2 and ω_2 .

Geometry	i_1	i_2	ω_1	ω_2
1/17	0	0	180	0
2/18	0	0	71	30
3/19	0	0	71	-30
4/20	0	0	71	90
5/21	-109	-60	180	0
6/22	-109	-60	71	30
7/23	-109	-60	71	-30
8/24	-109	-60	71	90
9/25	-109	0	180	0
10/26	-109	0	71	30
11/27	-109	0	71	-30
12/28	-109	0	71	90
13/29	-109	60	180	0
14/30	-109	60	71	30
15/31	-109	60	71	-30
16/32	-109	60	71	90

will be available under <http://www.usm.uni-muenchen.de>

Figure A3. Top: Velocity maps of the same 1:1 remnants like in the previous figure, but with the gas particles converted into stars. Bottom: Kinematic position angles as before. Overall misalignment is reduced, some KDCs are not visible anymore, as the gas dominates the center.

will be available under <http://www.usm.uni-muenchen.de>

Figure A4. The k_1 term (bulk rotation) and the k_5/k_1 (deviation from regular rotation) are plotted with a common x-axis. The low-rotation of 11C5, due to a high box orbit fraction in this remnant causes a high k_5/k_1 ratio.

will be available under <http://www.usm.uni-muenchen.de>

Figure A5. The k_1 (bulk rotation) profiles and the k_5/k_1 ratio for the stellar component of remnants with gaseous progenitors. Some CRCs are clearly visible in 11S6, 11S13, 11S14 and 11S16 in both a sudden peak in k_5/k_1 and in the double hump structure of k_1 .

will be available under <http://www.usm.uni-muenchen.de>

Figure A6. Velocity maps for the collisionless 3:1 remnants for the XZ projection.

will be available under <http://www.usm.uni-muenchen.de>

Figure A7. Velocity maps for the stellar component of the 3:1 remnants which had progenitors with a gas component

will be available under <http://www.usm.uni-muenchen.de>

Figure A8. Velocity maps of the same 3:1 remnants like in the previous figure but with the gas particles converted into stars